Hydrothermal instability and ground displacement at the Campi Flegrei caldera

A. P. Rinaldi[a,b,*], M. Todesco[a], M. Bonafede[b]

[a] *Istituto Nazionale di Geofisica e Vulcanologia, Sezione di Bologna, Italy*
[b] *Dipartimento di Fisica, Settore Geofisica, Università di Bologna, Italy*

Abstract

Ground deformation is commonly observed at active volcanoes, where it represents a reliable sign of unrest and a potential precursor of eruptive activity. The source of deformation, however, is not always unequivocally constrained. Magma ascent and differentiation are generally involved, but hydrothermal fluids may play a role, due to thermal expansion and pore pressure acting on rocks. The identification of mechanisms driving ground displacement bears important consequences for hazard evaluation. The aim of this work is to evaluate mechanical effects associated with pressurization and heating of hydrothermal fluids. We first simulate the heat and fluid flow driven by the arrival of magmatic fluids from greater depth. Then, we calculate the rock deformation arising from simulated pressure and temperature changes within a shallow hydrothermal system. We employ a mathematical model, based on the linear theory of thermo-poro-elasticity and on a system of distributed equivalent forces. Results show that stronger degassing of a magmatic source may cause several centimeters of uplift.

*Corresponding author

Email addresses: rinaldi@bo.ingv.it (A. P. Rinaldi), todesco@bo.ingv.it (M. Todesco), maurizio.bonafede@unibo.it (M. Bonafede)

1. Introduction

This research work stems from the recent evolution of the Campi Flegrei (CF) caldera (Italy): although the last eruption took place in 1538 AD, secondary activity has always been present and, in particular, changes of geochemical and geophysical parameters highlighted periods of unrest during the last 50 years. Ground deformation (or bradyseism) characterized these unrests, and more than 3 meters of uplift were recorded at the end of the two major episodes, in 1969-1971 and 1982-1984. A slow subsidence begun in 1985 and, since then, only minor uplifts (a few cm each) occurred in the caldera (De Natale et al., 2001). Each uplift phase has been accompanied by seismic activity and gravity changes, and followed by variation of discharge rate and gas composition in fumaroles. Minor crises were similar to the larger ones in terms of deformation pattern, compositional change and seismicity. Both large and small unrests have been carefully studied for their actual and potential consequences on the densely inhabited surrounding region. Early models ascribed the observed deformation to a pressure or volume change inside a magma chamber (Bonafede et al., 1986; Bianchi et al., 1987; De Natale et al., 1991). Casertano et al. (1976) made a pioneer study considering the importance of fluids in bradyseismic events. More recently, other authors recognized the effects of heating and expansion of hydrothermal fluids during an unrest (Bonafede, 1990, 1991; De Natale et al., 1991, 2001; Gaeta et al., 1998; Hurwitz et al., 2007; Hutnak et al., 2009; Orsi et al., 1999). The occurrence of seismicity in the CF caldera (Troise et al., 1997) and gravity changes (Bonafede and Mazzanti, 1998) were also modeled. These models describe the maximum uplift (1.8 m) observed in 1982-84, and authors suggest that the following subsidence could be due to lateral diffusion of fluids. Using a 1D model, Gaeta et al. (2003) explain minor uplifts as a consequence of hydrothermal fluid circulation. Although these models provide important conceptual insights, they are based on very simplified descriptions of the fluid dynamics and of the embedding medium.

The use of a more sophisticated model of hydrothermal circulation showed that several aspects of the complex unrest dynamics (including deformation) are related to the intensity of magmatic degassing (Chiodini et al., 2003; Todesco et al., 2003a,b, 2004; Todesco and Berrino, 2005).

The involvement of both magma and hydrothermal fluids in the recent evolution of the CF caldera was confirmed by further studies relating deformation and gravity data to the density of the source of deformation (Gottsmann et al., 2006; Amoruso et al., 2008; Bonafede and Ferrari, 2008).

In this work, we want to quantify the amount of deformation that can be caused by hydrothermal fluids during a generic unrest period at Campi Flegrei.

Following a well established approach (Todesco et al., 2003b, 2004; Hurwitz et al., 2007), we first simulate the evolution of the hydrothermal system; then we compute the deformation arising from the simulated changes in pore pressure and temperature.

Our simulation of hydrothermal circulation is based on a conceptual model that was developed for Campi Flegrei in previous papers (Chiodini et al., 2003; Todesco et al., 2003a,b, 2004; Todesco and Berrino, 2005): the hydrothermal system is fed by fluids of magmatic origin, and unrest events correspond to periods of increased magmatic degassing.

Pore pressure and temperature changes, arising from a given unrest event, are considered here as axially symmetric distributed sources of deformation, and described in terms of a system of equivalent forces. The resulting displacement of the ground surface is then computed analytically, according to the linear theory of thermo-poro-elasticity. Results show that the simulated unrest period can generate centimeters of vertical displacement at the free surface of an elastic homogeneous half-space.

2. The ground deformation model

The mathematical model presented here is based on the linear theory of poro-elasticity, which describes the elastic deformation of a porous medium taking into account the flow of a hot fluid that propagates through the pores. Here we follow the formulation proposed by Rice and Cleary (1976) and, given the high temperatures of the fluid, we also take into account the thermo-elastic response of the rock as described by McTigue (1986). The deformation e_{ij} due to a given change in pore pressure and temperature is:

$$e_{ij} = \frac{1}{2\mu}\left(\sigma_{ij} - \frac{\nu}{1+\nu}\sigma_{kk}\delta_{ij}\right) + \frac{\Delta p}{3H}\delta_{ij} + \frac{\alpha_s}{3}\Delta T\delta_{ij} \tag{1}$$

where σ_{ij} is the stress tensor; σ_{kk} is the trace of the stress tensor; μ is the shear modulus; ν is the Poisson's ratio in free-drainage conditions; $1/H = 1/K - 1/K'_s$ is the Biot's constant (K is the isothermal, drained bulk modulus and K'_s is the bulk modulus of the solid constituent); α_s is the volumetric thermal expansion coefficient for the solid matrix; δ_{ij} is the Kronecker delta. Δp and ΔT are the pore pressure and temperature changes, respectively.

In order to evaluate the displacement field arising from pressure and temperature changes at a given point, we follow the approach proposed by Aki and Richards (1980) to compute the seismic displacement generated by a volume source.

We first consider a porous medium in an initial configuration of vanishing stress and strain. We identify a volume source, with dimensions dx, dy, dz, and remove it from its surrounding, without affecting the porous matrix. We then increase pore pressure and temperature in the source volume by supplying heat and fluid, at constant (vanishing) stress. At this stage (A), the source remains unstressed ($\tau_{ij}^{(A)} = 0$), but its volume is isotropically strained ("*Aki's stress-free strain*") by an amount:

$$e_{ij}^{(A)} = \frac{1}{3}\Delta\theta\delta_{ij}$$

where $\Delta\theta$ is the relative volume change, given by the trace of the strain tensor (1)

$$\Delta\theta = \frac{\Delta V}{V_0} = e_{kk}^{(A)} = \frac{\Delta p}{H} + \alpha_s \Delta T$$

In order to place the source back in its original position in the porous medium (stage B), we need to restore its original volume V_0: we apply a stress field $\tau_{ij}^{(B)} = -K\Delta\theta\delta_{ij}$ at constant pore pressure and temperature, to obtain a deformation $e_{ij}^{(B)} = -e_{ij}^{(A)}$:

$$\tau_{ij} = \tau_{ij}^{(A)} + \tau_{ij}^{(B)} = \tau_{ij}^{(B)}, \qquad e_{ij} = e_{ij}^{(A)} + e_{ij}^{(B)} = 0$$

Now the source is back in its place, but a traction discontinuity exists over its surface: the matrix is still unstressed and unstrained while the source is subject to the artificial "stress glut" τ_{ij} applied to restore its initial volume. The difference between the outer and the inner values of traction is then

$-\tau_{ij}n_j$. Removal of this traction discontinuity will cause the source to expand again but, this time, the surrounding matrix acts against the expansion and prevents the source from reaching the stress-free volume. The displacement field due to the applied pressure and temperature changes at the source can be expressed in terms of this traction discontinuity (Aki and Richards, 1980):

$$u_i(\mathbf{x}) = \int_V K\Delta\theta(\mathbf{x}')\mathcal{G}_{ik,k}(\mathbf{x},\mathbf{x}')\,\mathrm{d}x'\,\mathrm{d}y'\,\mathrm{d}z' \tag{2}$$

where K is the bulk modulus, $\mathbf{x}$ is the observation point, $\mathbf{x}'$ is the source position and $\mathcal{G}_{ik}$ is the Green's Tensor.

In order to evaluate the divergence of the Green's Tensor we use a system of distributed equivalent forces. The isotropic point source can be mathematically described as a system of three equal orthogonal dipoles placed at the source point (Wang, 2000). The displacement field $\mathcal{G}_{ik}$ arising from a single force in a homogeneous half-space with a traction-free boundary was provided by Mindlin (1936).

In this work, we first calculate the displacement due to a single dipole set along the $\hat{x}$, $\hat{y}$ or $\hat{z}$ axes, and then we sum the single components of each field in order to have the total displacement at the observation point. The vertical component of the displacement for this case is:

$$\begin{aligned} u_z^{tot} = Fh\frac{(1-2\nu)}{8\pi\mu(1-\nu)}&\left[\frac{(z-z')}{R_1^3}+\right.\\ &\left.-(3-4\nu)\frac{z+z'}{R_2^3}+\frac{2z}{R_2^3}-\frac{6z(z+z')^2}{R_2^5}\right] \end{aligned} \tag{3}$$

where F and h are the intensity and arm of each dipole; $(x,\ y,\ z)$ is the observation point and $(x',\ y',\ z')$ is the source point; R_1 is the distance between the deformation source and the observation point ($R_1^2 = (x-x')^2 + (y-y')^2 + (z-z')^2$) and R_2 is the distance between the mirror-source and the observation point ($R_2^2 = (x-x')^2 + (y-y')^2 + (z+z')^2$).

Since we are using a free surface calculation, the horizontal component of the displacement wil be different than the vertical:

$$u_r^{tot} = Fh\frac{(1-2\nu)}{8\pi\mu(1-\nu)}\left[\frac{1}{R_1^3}+ \right.$$
$$\left. -(3-4\nu)\frac{1}{R_2^3} - \frac{6z(z+z')}{R_2^5}\right](r-r') \tag{4}$$

where $r^2 = x^2 + y^2$ and $r'^2 = x'^2 + y'^2$ represent the radial distance of the observation point and of the source from the $\hat{z}$ axes, respectively.

3. The fluid flow model

Hydrothermal circulation is simulated with the multi-phase and multi-component TOUGH2 model (Pruess et al., 1999), which describes the coupled flow of heat and fluids through the porous medium. In the present application, the considered fluid components are water and carbon dioxide. The computational domain, two-dimensional and axisymmetric, is 10 km wide and 1.5 km deep (Fig. 1 shows the domain up to 1 km, since most of changes happen near the symmetry axis).

Bottom and side boundaries are impervious and adiabatic. Atmospheric conditions are fixed along the upper boundary, which is open to heat and fluid flows. The properties of the porous medium are listed in Table 1. The shallow hydrothermal circulation is driven by the injection of a hot (ca. 623 K) mixture of water and carbon dioxide. This mixture represents the magmatic component that enters the domain near the symmetry axis (Fig. 1).

Initial conditions are obtained by simulating a long-lasting (i.e.: thousands of years) injection of magmatic fluids. The prescribed flow rate at the inlet (1000 tons/day of CO_2 and 2400 tons/day of H_2O) reflects data collected at the CF caldera, and corresponds to a CO_2/H_2O molar ratio of 0.17 (Chiodini et al., 2003). As described in previous works (Chiodini et al., 2003; Todesco et al., 2003a,b, 2004), the prolonged activity of the fluid source generates, at the steady state, a wide two-phase plume, with a shallow single-phase gas region (Fig. 1a). High temperature characterizes the entire plume (Fig. 1b), which is also slightly pressurized with respect to the hydrostatic gradient.

Starting from these steady-state initial conditions, the simulation presented here describes an initial unrest phase, provided by a sudden increase of fluid flow, followed by a longer quiet period. The unrest phase lasts 20 months, during which both the input of magmatic fluids and the carbon dioxide content increase (6000 tons/day of CO_2 and 6100 tons/day of H_2O, $CO_2/H_2O=0.4$) at same, constant input temperature (ca. 623 K). During the following quiet phase, flow rate and composition return to the initial values. Inlet conditions corresponding to the different phases are listed in Table 2. A sequence of similar unrest and quiet periods was shown to be consistent with observed changes in gas composition and gravity at the CF caldera during the last 30 years (Chiodini et al., 2003; Todesco and Berrino, 2005).

The imposition of a larger discharge rate during the unrest is accompanied by a pressure build-up, which gradually spreads out as the fluids propagate through the system. At the end of the unrest, pressure changes range from +5 MPa, near the fluid inlet, to +0.1 MPa near the ground surface (Fig. 2a).

The unrest is also associated with temperature changes, even if the specific enthalpy of injected fluids does not changes. Temperature changes, up to tens of Kelvin, are mostly confined along the edges of the two-phase plume (Fig. 2b). Most of these temperature changes are related to the lateral spreading of the two-phase region during the unrest. As the hot, gas-rich fluids replace the colder liquid water, temperature may increase up to 40 K (Fig. 3a). Temperature changes within the two-phase plume may occur as well, as a consequence of water phase changes: pressure build-up near the inlet can cause the condensation of water vapor (Fig. 3a) and the associated release of latent heat increases the temperature in the region above the fluid source (+5 K). At shallower depths, some fraction of liquid water in the two-phase region evaporates (Fig. 3a), subtracting latent heat and causing minor cooling (ca. -1.5 K).

When the unrest is over, pore pressure drops and the two-phase plume begins to shrink gradually. Decompression enhances water evaporation and associated cooling. Fluids entered during the unrest still propagate upwards, affecting shallower portions of the domain during the quiet (Fig. 3b). At the end of the simulation, pressure and temperature anomalies persist: localized overpressure (up to +0.1 MPa) is still present at shallow depth ($<$ 200 m), while most of the domain undergoes decompression (up to -0.3 MPa), particularly near the plume border (Fig. 2c). Temperature anomalies are mostly confined along the edges of the two-phase plume (Fig. 2d). A slow temperature decline occurs at depth, where heating (+20 K) still persists at the end of the simulation. Moderate heating (a few K) takes place at shallower depths, as hot fluids rise toward the surface (Fig. 3). The heated region is not uniform along the plume due to the competing effects of fluid displacement and phase changes during the simulation (Fig. 2d). It is interesting to note that pressure and temperature changes affect different regions of the domain, which do not necessarily reflect the position of the inlet of magmatic fluids (i.e. the location of the "source" that drives the unrest, Fig. 1).

4. Resulting displacement

To compute the vertical ground displacement arising from the simulated evolution, each element of the computational domain is considered as a potential source of deformation. Pressure and temperature changes at different times are calculated with respect to the initial pressure and temperature values in each element. The corresponding vertical displacement can be computed from the contribution of each element (el) of the grid (5):

$$\begin{aligned} u_z^{el} = -\frac{(1+\nu)}{12\pi(1-\nu)}\Delta\theta^{el}V^{el}\Bigg[&\frac{(z-z^{el})}{R_1^3}+ \\ &-(3-4\nu)\frac{z+z^{el}}{R_2^3}+\frac{2z}{R_2^3}-\frac{6z(z+z^{el})^2}{R_2^5}\Bigg] \end{aligned} \tag{5}$$

where $\Delta\theta^{el} = \left(\Delta p^{el}/H + \alpha_s \Delta T^{el}\right)$ represent the dilatation (compression) of a single element of the grid. V^{el} and z^{el} are the volume and depth of the element. R_1 and R_2 are the distance of the observation point from the element and from the image-element. The total displacement is calculated by summing the contributions of all grid block.

Contrary to previous works (Todesco et al. (2004); Hurwitz et al. (2007)), our approach for the computation of ground deformation does not require the specification of arbitrary boundary conditions over the boundary of the computational domain, since Mindlin's solutions provide vanishing stress over the free surface and vanishing displacements and stress at remote distance.

For the moment, we do not account for the effects of rock deformation back onto fluid propagation (full coupling).

The temporal evolution of ground displacement, calculated at the surface, on the symmetry axis, is shown in Figure 4a. The values for thermo-poro-elastic parameters are listed in Table 3. Uplift begins as soon as the injection rate is increased, at the beginning of the unrest, and reaches the maximum value (9 cm) at the end of the crisis. The quiet period is characterized by a slow subsidence that reflects the lower inflow of magmatic fluids. The minimum ground elevation (-1 cm) is attained at the end of the simulation. This trend of deformation arises from the temporal evolution of pressure and temperature anomalies (Fig. 4b). The faster uplift phase is due to the combined effects of increasing average pressure and temperature. When the unrest is over, the average pressure quickly declines, but the average temperature keeps increasing until hot fluids begin to discharge at the surface. The effects of fast decompression are therefore mitigated by thermal expansion, and the resulting subsidence rate is slower than the uplift rate.

The radial distribution of ground uplift, calculated at different times, is shown in Figure 5. At the end of unrest, the pattern of deformation is similar to a Mogi-type source (Mogi, 1958): the maximum uplift is right above the source and deformation is mostly confined within 4 km from the symmetry axis (Fig. 5a). A different pattern characterizes the subsidence. With time, changes along the border of the plume become shallower (Fig. 2), and some spikes in vertical displacement develop at 500-700 m from the symmetry axis. At the end of simulation (Fig. 5b), minor subsidence affects the axial region, and vertical displacement vanishes within the first 2 km.

The temporal evolution of vertical displacement does not depend only on the dynamics of the hydrothermal fluids. The mechanical properties of the porous rock control both the magnitude and the temporal evolution of ground deformation. This is a relevant aspect, as mechanical properties may change significantly with rock type and physical condition, and site-specific values are often poorly constrained. The effects of different values of bulk and shear moduli are shown in Figure 6. Increasing the bulk modulus reduces the uplift during the unrest, and leads to a slower subsidence during the quiet. For K values above 15 GPa, the initial ground elevation is not restored within the simulation time. Lower bulk moduli lead to larger vertical displacement during the unrest, and drive ground subsidence below the initial elevation. Differences in ground displacement scale quite linearly with increasing bulk modulus during the uplift: 5 GPa changes in bulk modulus produce about 1,5 cm difference in ground displacement (Fig. 6a). This linearity is conserved to the end of simulation, although following a different pattern. The shear modulus of the rocks also has a substantial effect on ground deformation. Low rock rigidity leads to larger vertical displacement (up to 18 cm) and faster subsidence during the quiet. In this case, displacements do not scale linearly with increased rigidity (Fig. 6b).

Bulk modulus K_s' changes, within the range 20-40 GPa, and thermal expansion coefficient changes, within the range 10^{-7}-10^{-5} K^{-1}, have minor effect on the maximum calculated ground displacements.

5. Conclusion

In this work we present a model of ground deformation based on the linear theory of thermo-poro-elasticity. The model was applied to compute the vertical ground displacement associated with heating and pressurization of hydrothermal fluids during an unrest event at the CF caldera. The evolution of the hydrothermal system was simulated with the TOUGH2 numerical code (Pruess et al., 1999). Then, the corresponding ground deformation was calculated under the assumption of homogeneous mechanical properties of the porous medium. Our approach does not require the definition of boundary conditions for the displacement along the periphery of the computational domain. This is particularly relevant in a small system such as ours, where the presence of a shallow bottom boundary certainly affects the mechanical response of the free surface.

Results show that increasing the fluid injection rate in our system (by a factor 3.5) leads to a maximum uplift of the order of 10 cm, which may double depending on the choice of mechanical properties of the porous rock. A slow subsidence takes place during the quiet phase, when hot fluids reach shallower depths and heating mitigates the effects of pressure drop, leading to a slower evolution.

The evolution of the two-phase region during the quiet is associated with a complex pattern of ground deformation along the surface, with peak values characterizing the edges of the plume. A complex radial pattern of deformation was already emphasized by Todesco et al. (2004)

A direct comparison with previous results (Todesco et al., 2003b, 2004) is not possible, due to a different choice of rock properties and inlet conditions. Nevertheless, results obtained by Todesco et al. (2003b), with a fivefold increase of the flow rate at the inlet, indicate a maximum uplift (15 cm) of the same order of magnitude.

The calculated displacements reflects the flow rate at the inlet, and the permeability of the system, which directly controls the pressure build-up and heat propagation. Stronger inputs of magmatic fluids would cause larger uplifts. Similarly, different choices of rock permeability (or any change in permeability during the unrest) are going to affect system conditions and its response to unrest periods. Higher permeability favors fluid propagation, and hence heating of the system but, at the same time, reduces pressure build up. On the contrary, low permeability hinders fluid propagation and favors the pressure increase, which however would remain confined within a smaller region. The overall outcome in terms of ground displacement is difficult to estimate and further research should focus on this aspect.

Initial conditions also play a role: the deformation depends on pressure and temperature changes with respect to the initial conditions. The same input of magmatic fluids entering a colder region would cause much larger vertical displacement. If the system becomes heated by subsequent unrest events, as in the case of CF, ground deformation is expected to become progressively less pronounced over time, even if the input of magmatic fluids is unchanged. The remarkable difference between the large and the small unrest events at the CF caldera could be due to different sources of deformation acting at different times, but it could also derive from significant changes in rock properties and system conditions after the first major episodes.

With the present choice of initial conditions, feeding rate, and rock properties, based on a sound conceptual model that was developed for CF over time, the calculated displacement is consistent with the deformation observed during the recent, minor uplift events at CF. Our results therefore support the importance of hydrothermal fluids in these recent episodes. The strong influence of system properties and conditions on the calculated deformation pattern should be carefully considered when trying to infer properties of the deformation source from the observed pattern of ground displacement.

References

Aki, K., and P. G. Richards (1980), Quantitative Seismology - Theory and Methods, vol. 1, W. H. Freeman & Co., San Francisco, California, USA.

Amoruso, A., L. Crescentini, and G. Berrino (2008), Simultaneous inversion of deformation and gravity changes in a horizontally layered half-space: Evidences for magma intrusion during 1982-1984 unrest at Campi Flegrei caldera (Italy), Earth Planet. Sci. Lett., 272, 181–188, doi: 10.1016/j.epsl.2008.04.040.

Bianchi, R., A. Coradini, C. Federico, G. Giberti, P. Lanciano, J. P. Pozzi, G. Sartoris, and R. Scandone (1987), Modeling of surface deformation in volcanic areas: The 1970-1972 and 1982-1984 crises of Campi Flegrei, Italy, J. Geophys. Res., 92(B13), 14,139–14,150.

Bonafede, M. (1990), Axi-symmetric deformation of a thermo-poro-elastic half-space: inflation of a magma chamber, Geophys. J. Int., 103, 289–299.

Bonafede, M. (1991), Hot fluid migration: an efficient source of ground deformation: application to the 1982-1985 crisis at Campi Flegrei-Italy, J. Volcanol. Geotherm. Res., 48, 187–198.

Bonafede, M., and C. Ferrari (2008), Analytical models of deformation and residual gravity changes due to a Mogi source in a viscoelastic medium, Tectonophys., in press, doi: 10.1016/j.tecto.2008.10.006.

Bonafede, M., and M. Mazzanti (1998), Modelling gravity variations consistent with ground deformation in the Campi Flegrei caldera (Italy), J. Volcanol. Geotherm. Res., 81, 137–157.

Bonafede, M., M. Dragoni, and F. Quareni (1986), Displacement and stress fields produced by a centre of dilatation and by a pressure source in a viscoelastic half-space: application to the study of ground deformation and seismic activity at Campi Flegrei, Italy, Geophys. J. R. astr. Soc., 87, 455–485.

Casertano, L., A. Oliveri del Castillo, and M. T. Quagliariello (1976), Hydrodynamics and geodynamics in the Phlegrean fields area of Italy, Nature, 264, 161–164.

Chiodini, G., M. Todesco, S. Caliro, C. D. Gaudio, G. Macedonio, and M.Russo (2003), Magma degassing as a trigger of bradyseismic events: the case of Phlegrean fields (Italy), Geophys. Res. Lett., 30(8), 1434–1437.

De Natale, G., F. Pingue, P. Allard, and A. Zollo (1991), Geophysical and geochemical modelling of the 1982-1984 unrest phenomena at Campi Flegrei caldera (southern Italy), J. Volcanol. Geotherm. Res., 48, 199–222.

De Natale, G., C. Troise, and F. Pingue (2001), A mechanical fluid-dynamical model for ground movements at Campi Flegrei caldera, J. Geodyn., 32, 487–571.

Gaeta, F. S., G. D. Natale, F. Peluso, G. Mastrolorenzo, D. Castagnolo, C. Troise, F. Pingue, D. G. Mita, and S. Rossano (1998), Genesis and evolution of unrest episodes at Campi Flegrei caldera: The role of thermal fluid-dynamical processes in the geothermal system, J. Geophys. Res., 103(B9), 20,921–20,933.

Gaeta, F. S., F. Peluso, I. Arienzo, D. Castagnolo, G. De Natale, G. Milano, C. Albanese, and D. G. Mita (2003), A physical appraisal of a new aspect of bradyseism: The miniuplifts, J. Geophys. Res., 108(B8), doi: 10.1029/2002JB001913.

Gottsmann, J., A. Folch, and H. Rymer (2006), Unrest at Campi Flegrei: A contribution to the magmatic versus hydrothermal debate from inverse and finite element modelling, J. Geophys. Res., 111, B07203, doi: 10.1029/2005JB003745.

Hurwitz, S., L. B. Christiansen, and P. A. Hsieh (2007), Hydrothermal fluid flow and deformation in large calderas: Inferences from numerical simulations, J. Geophys. Res., 112, B02206, doi:10.1029/2006JB004689.

Hutnak, M., S. Hurwitz, S. E. Ingebritsen and P. A. Hsieh (2009), Numerical models of caaldera deformation: Effects of multiphase and multicomponent hydrothermal fluid flow, J. Geophys. Res., 114, B04411, doi: 10.129/2008JB006151.

McTigue, D. F. (1986), Thermoelastic response of fluid-saturated porous rock, J. Geophys. Res., 91(B9), 9533–9542.

Mogi, K. (1958), Relations between the eruption of various volcanoes and the deformation of the ground surface around them, Bull. Earthquake Res. Inst. Univ. Tokyo, 36, 99-134.

Mindlin, R. D. (1936), Force at a point in the interior of a semi-infinite solid, Physics, 7, 39–44.

Orsi, G., S. M. Petrazzuoli, and K. Wohletz (1999), Mechanical and thermo-fluid behaviour during unrest at the Campi Flegri caldera (Italy), J. Volcanol. Geotherm. Res., 91, 453–470.

Pruess, K., C. Oldenburg, and G. Moridis (1999), TOUGH2 user's guide, version 2.0, Paper LBNL-43134, Lawrence Berkeley Natl. Lab., Berkeley, CA, USA.

Rice, J. R., and M. P. Cleary (1976), Some basic stress diffusion solutions for fluid-saturated elastic porous media with compressible constituents, Rev. Geophys. Space Phys., 14, 227–241.

Todesco, M., and G. Berrino (2005), Modelling hydrothermal fluid circulation and gravity signals at the Phlegrean Fields caldera, Earth Plan. Sci. Lett., 240, 328–338.

Todesco, M., G. Chiodini, and G. Macedonio (2003), Monitoring and modelling hydrothermal fluid emission at La Solfatara (Phlegrean Field, Italy). An interdisciplinary approach to the study of diffuse degassing, J. Volcanol. Geotherm. Res., 125, 57–79.

Todesco, M., J. Rutqvist, K. Pruess, and C. M. Oldenburg (2003b), Multiphase fluid circulation and ground deformation: a new perspective on bradyseismic activity at the Phlegrean Fields (Italy). In: Proceedings of the 28^{th} Workshop on Geothermal Research Engineering, Stanford, CA, USA.

Todesco, M., J. Rutqvist, G. Chiodini, K. Pruess, and C. M. Oldenburg (2004), Modeling of recent volcanic episodes at Phlegrean Fields (Italy): geochemical variations and ground deformation, Geothermics, 33, 531–547.

Troise, C., G. D. Natale, and F. Pingue (1997), A model for earthquake generation during unrest episodes at Campi Flegrei and Rabaul calderas, Geophys. Res. Lett., 24(13), 1575–1578.

Wang, H. F. (2000), Theory of Linear Poroelasticity with Applications to Geomechanics and Hydrology, 276 pp., Princeton University Press, Princeton and Oxford.

Density	2000 kg m^{-3}
Permeability	10^{-14} m^2
Porosity	0.20
Conductivity	2.80 W m^{-1} K^{-1}
Specific Heat	1000 J kg^{-1} K^{-1}

Table 1: Rock properties considered in the simulation of the hydrothermal system. These properties remain constant during the simulation.

	CO_2	**H_2O**	**Molar Ratio**
Quiet	1000	2400	0.17
Unrest	6000	6100	0.40

Table 2: Flow rate (ton/day) and CO_2/H_2O molar ratio at the inlet during the unrest and the following quiet. The enthalpy of injected fluids correspons to a temperature of ca. 623 K and does not change during the simulation.

μ	2 GPa
K	5 GPa
K'_s	30 GPa
α_s	10^{-5} K^{-1}

Table 3: Rock mechanical properties considered in the computation of the vertical ground displacement. μ is the shear modulus, K is the drained bulk modulus, K'_s is the bulk modulus of the solid constituent and α_s is the volumetric thermal expansion coefficient for the solid matrix.

Figure 1: Initial conditions: a) volumetric gas fraction and b) temperature (K).The star indicates the inlet of magmatic fluids, which has a radius of 150 m. The computational domain was discretized into 2580 elements, with radial dimensions ranging from 25 to 3196 m and thickness from 5 to 25 m.

Figure 2: Simulated changes with respect to the initial conditions at different times: a,c) pore pressure (MPa) and b,d)temperature (K) changes at the end of unrest and at the end of simulation, respectively. The figures refer to axial region. The star indicates the inlet of magmatic fluids.

Figure 3: Simulated changes with respect to the initial conditions: volumetric gas fraction at the end of unrest (a) and at the end of simulation (b). Arrows describe the pattern of flow for the liquid (black) and gas phase (magenta).

Figure 4: (a) Temporal evolution of vertical ground displacement at the symmetry axis. (b) Temporal variation of the average temperature (solid line) and average pore pressure (dashed line). Values are computed over the entire domain and normalized with respect to the maximum value. Shaded area in both figures highlights the unrest period. Rock mechanical properties: μ=2 GPa; K=5 GPa; K_s'=30 GPa; α=10^{-5} K^{-1}

Figure 5: Radial distribution of vertical ground displacement, at the end of the unrest (a), and at later times (b).

Figure 6: Temporal evolution of vertical ground displacement at the simmetry axis for differet values of the rigidity (a) and bulk modulus (b). The other parameters are as listed in Table 3. Shaded are in both figures highlights the unrest period.

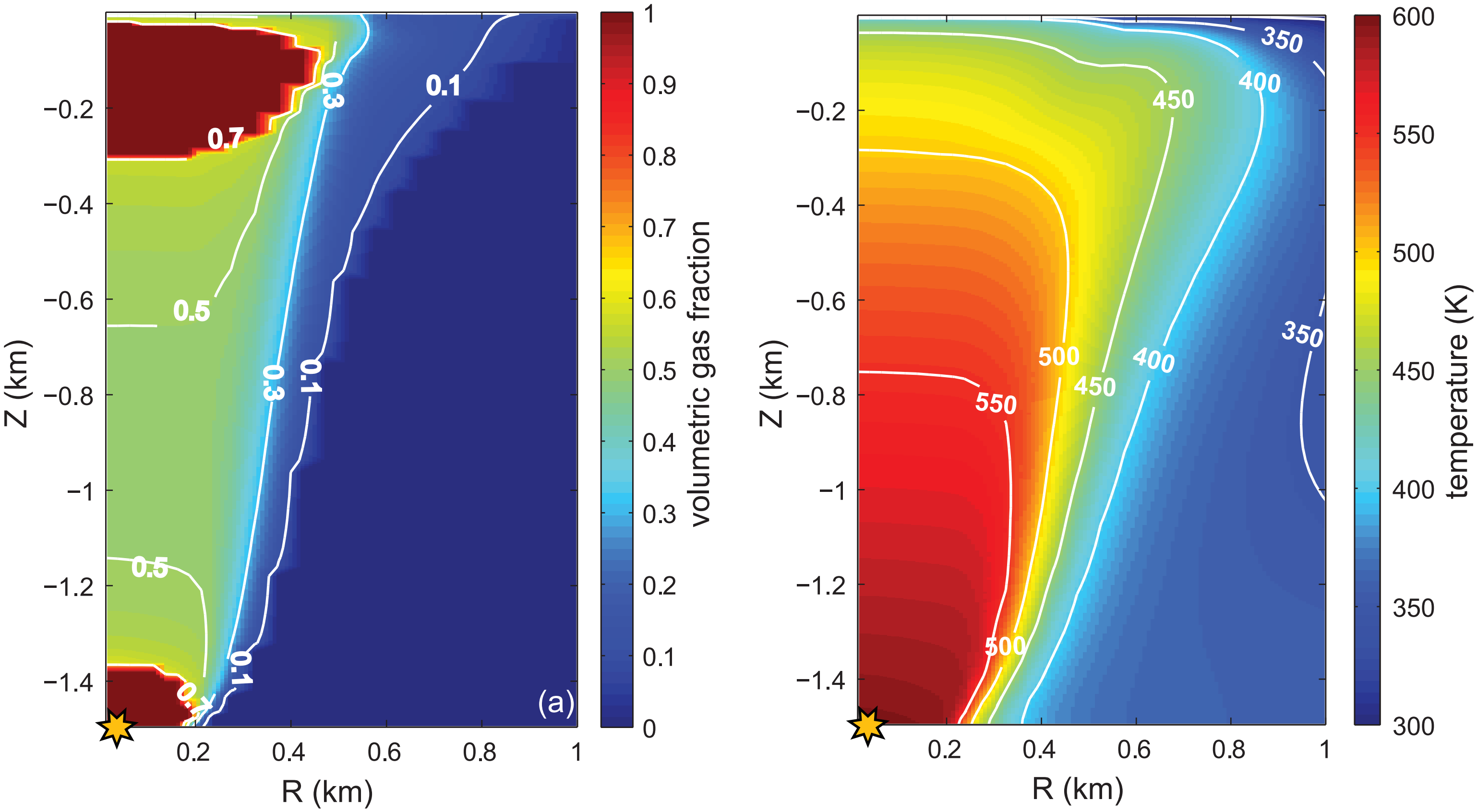

Z (km)
R (km)
volumetric gas fraction
(a)
temperature (K)

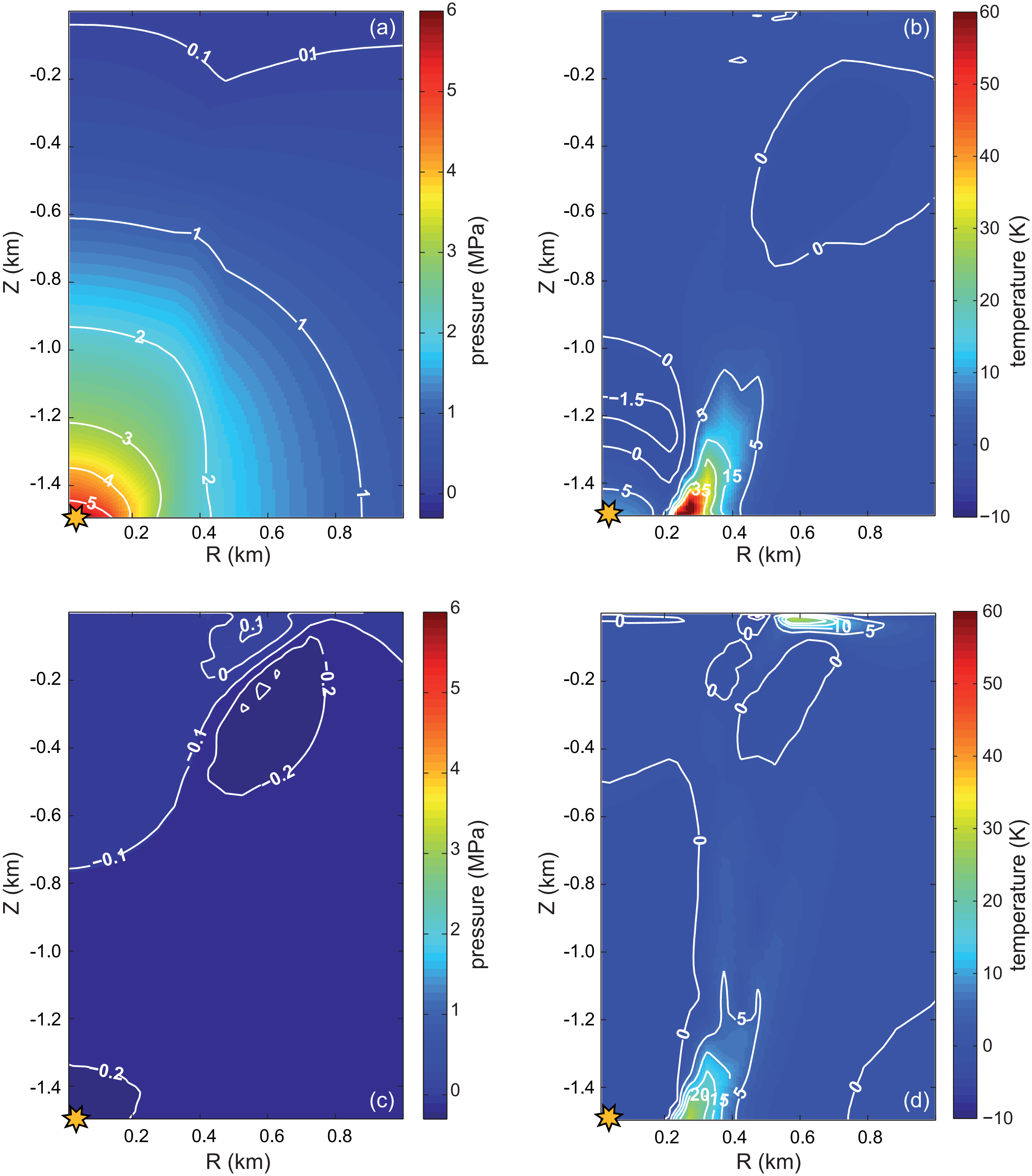
(a)
(b)
(c)
(d)
Z (km)
R (km)
pressure (MPa)
temperature (K)
-0.2
-0.4
-0.6
-0.8
-1.0
-1.2
-1.4
0.2
0.4
0.6
0.8
0.1
01
1
2
3
4
5
0
-0.1
-0.2
-1.5
15
35
20
10
6
60
50
40
30
-10

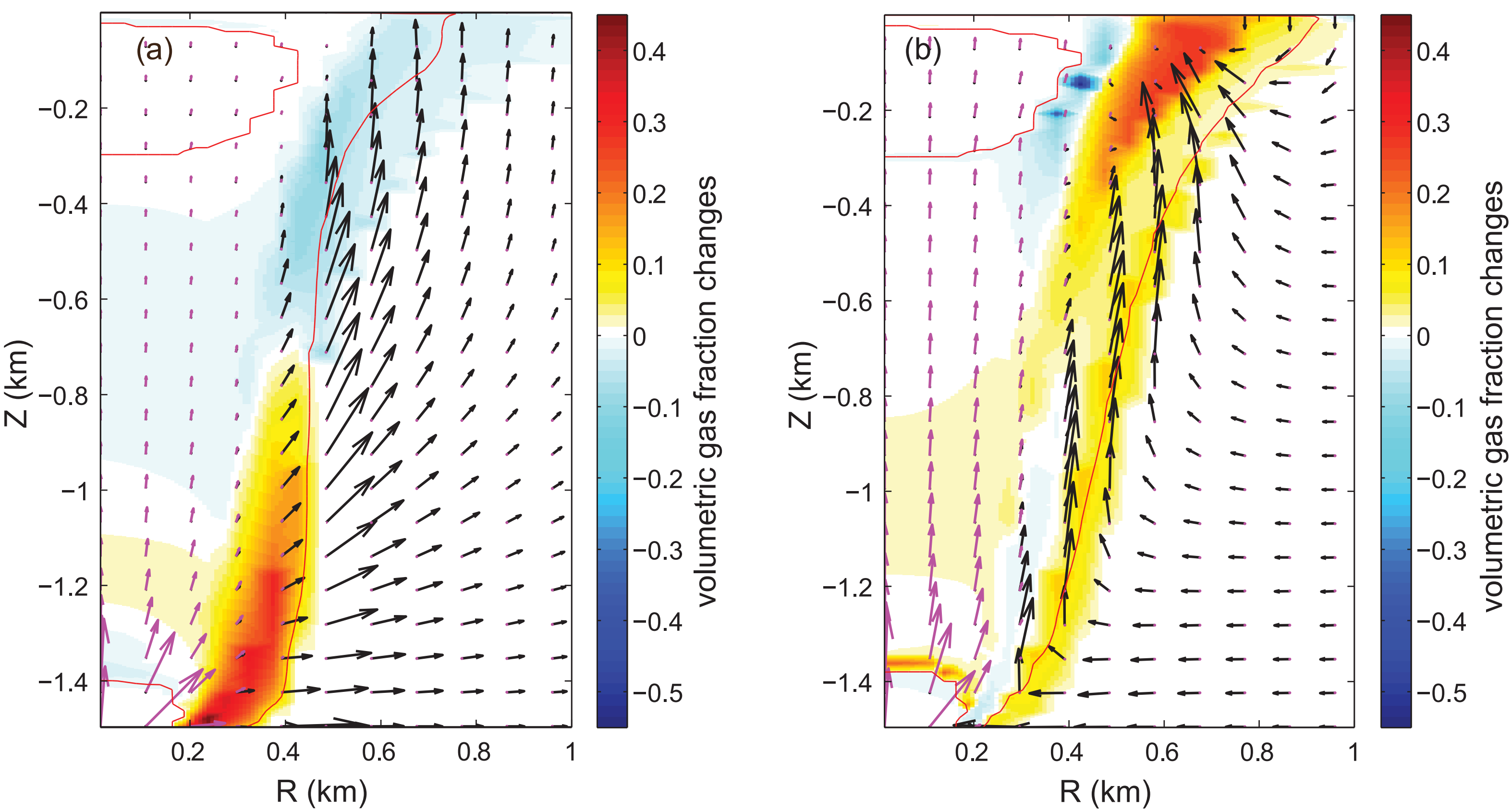

(a)
(b)
Z (km)
R (km)
volumetric gas fraction changes
−0.2
−0.4
−0.6
−0.8
−1
−1.2
−1.4
0.2
0.4
0.6
0.8
1
0.4
0.3
0.2
0.1
0
−0.1
−0.2
−0.3
−0.4
−0.5

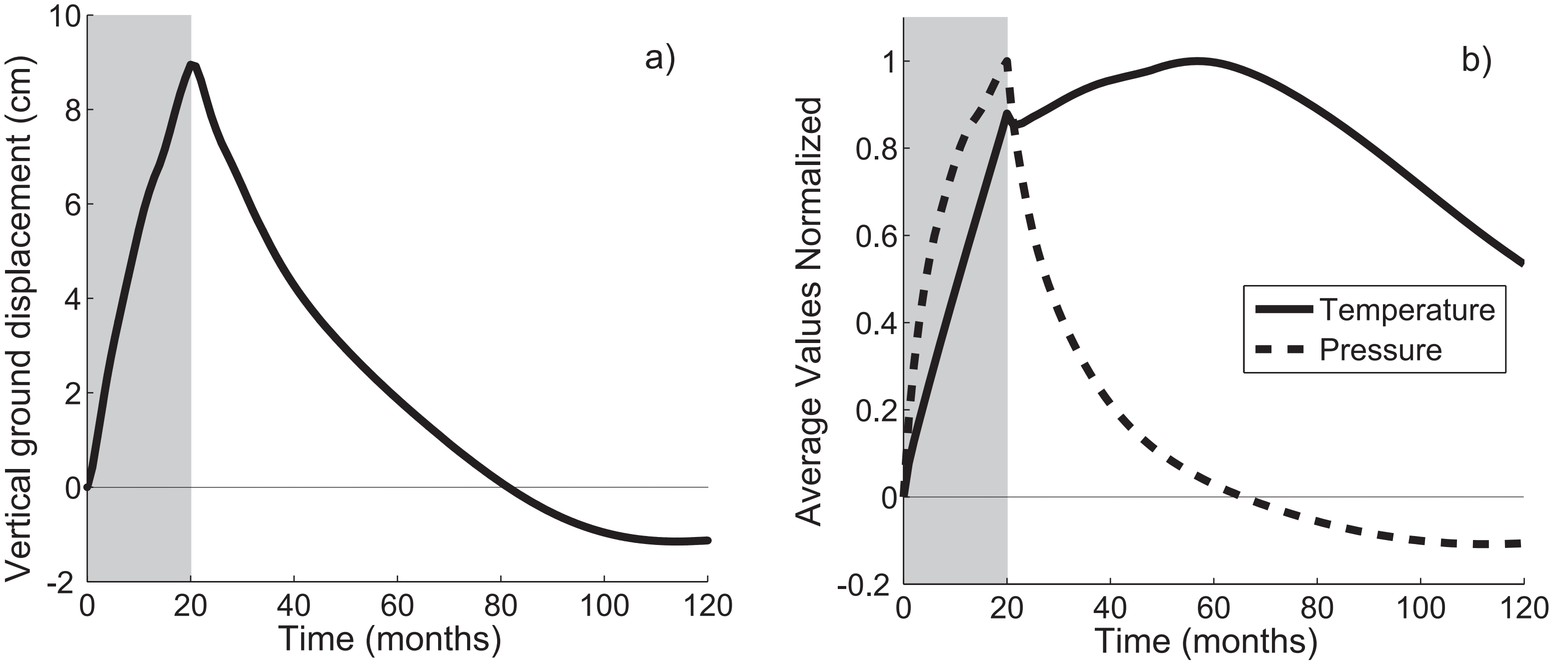

a)
Vertical ground displacement (cm)
Time (months)
-2
0
2
4
6
8
10
0
20
40
60
80
100
120
b)
Average Values Normalized
Time (months)
-0.2
0
0.2
0.4
0.6
0.8
1
Temperature
Pressure

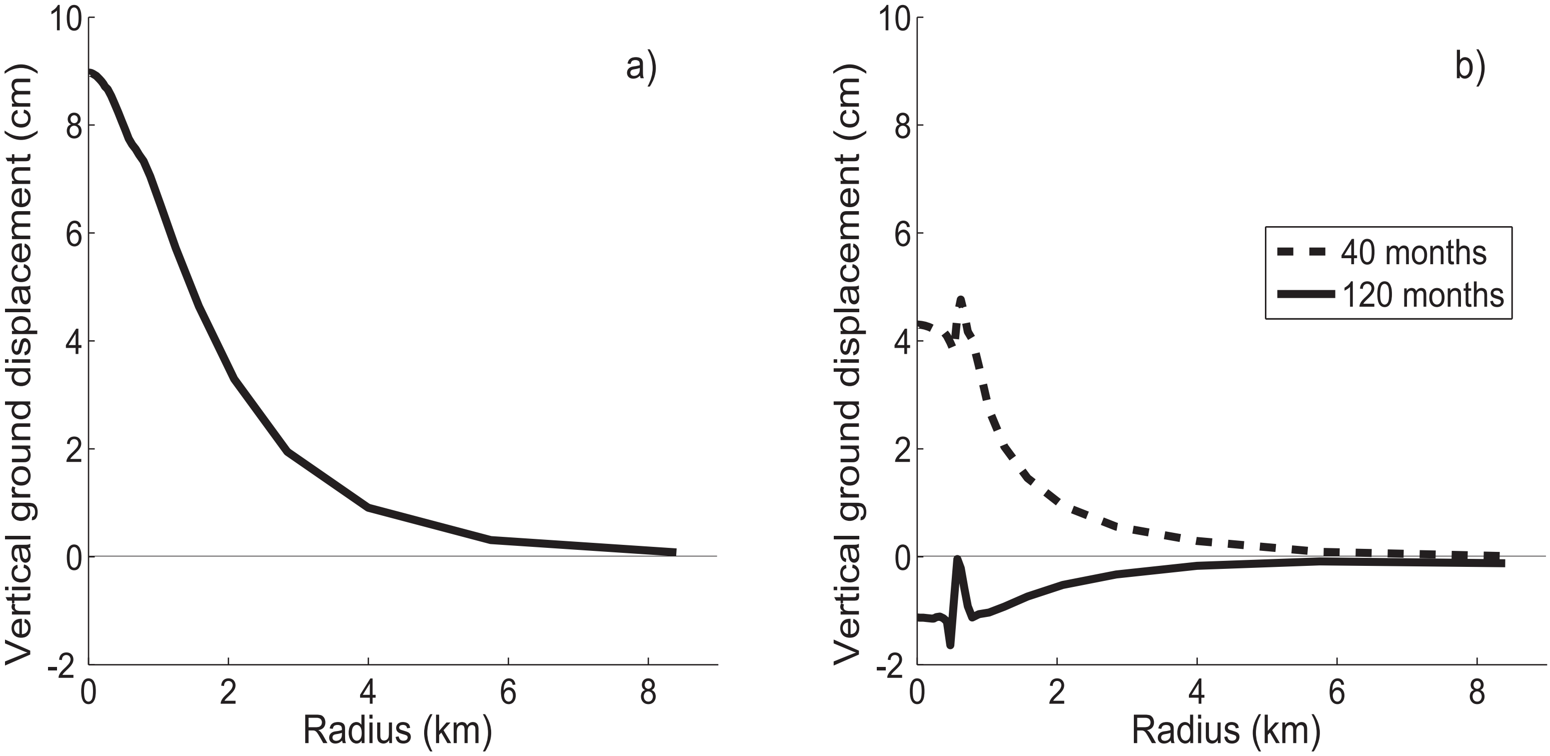
a)
b)
Vertical ground displacement (cm)
Radius (km)
40 months
120 months
10
8
6
4
2
0
-2
0
2
4
6
8

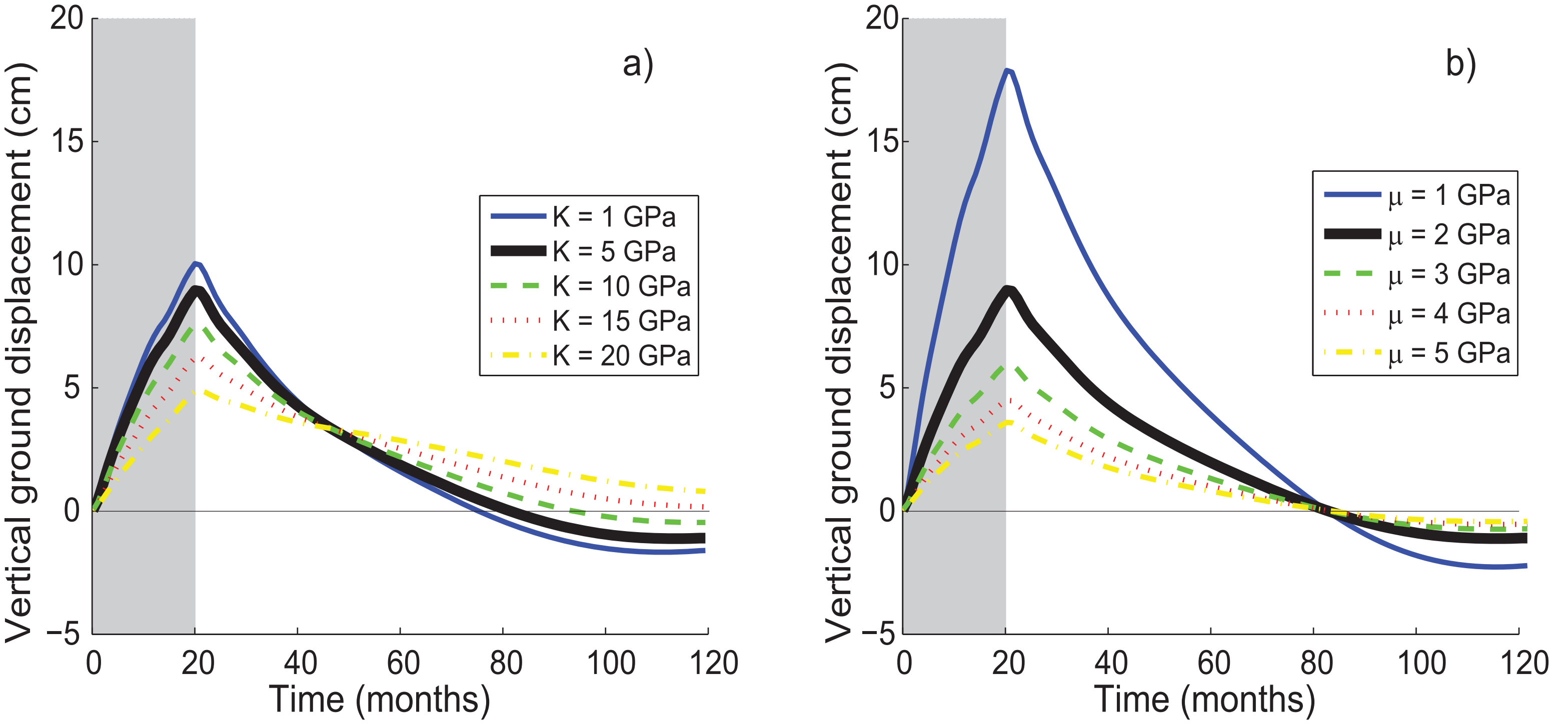

a)
Vertical ground displacement (cm)
Time (months)
K = 1 GPa
K = 5 GPa
K = 10 GPa
K = 15 GPa
K = 20 GPa
b)
μ = 1 GPa
μ = 2 GPa
μ = 3 GPa
μ = 4 GPa
μ = 5 GPa
20
15
10
5
0
−5
0
20
40
60
80
100
120